ACS APPLIED MATERIALS & INTERFACES

www.acsami.org

Research Article

Macroscopic Au@PANI Core/Shell Nanoparticle Superlattice Monolayer Film with Dual-Responsive Plasmonic Switches

Han Lin, Liping Song, Youju Huang,* Qian Cheng, Yanping Yang, Zhiyong Guo,* Fengmei Su, and Tao Chen*

Cite This: *ACS Appl. Mater. Interfaces* 2020, 12, 11296−11304

Read Online

ACCESS | Metrics & More | Article Recommendations | Supporting Information

ABSTRACT: The self-assembled gold nanoparticle (NP) superlattice displays unusual but distinctive features such as high mechanical and free-standing performance, electrical conductivity, and plasmonic properties, which are widely employed in various applications especially in biological diagnostics and optoelectronic devices. For a two-dimensional (2D) superlattice monolayer film composed of a given metal nanostructure, it is rather challenging to tune either its plasmonic properties or its optical properties in a reversible way, and it has not been reported. It is therefore of significant value to construct a free-standing 2D superlattice monolayer film of gold nanoparticles with an intelligent response and desired functions. Herein, we developed an easy and efficient approach to construct a gold nanoparticle superlattice film with a dual-responsive plasmonic switch. In this system, gold nanoparticles were coated by polyaniline (PANI) and then interracially self-assembled into a monolayer film at the air−liquid interface. The PANI shell plays two important roles in the superlattice monolayer film. First, the PANI shell acts as a physical spacer to provide a steric hindrance to counteract the van der Waals (vdW) attraction between densely packed nanoparticles (NPs), resulting in the formation of a superlattice by adjusting the thickness of the PANI shell. Second, the PANI shells provide the superlattice film with multiple stimuli such as electrical potential and pH change, leading to reversible optical and plasmonic responsiveness. The superlattice monolayer film can show a vivid color change from olive green to pink, or from olive green to violet by the change of the corresponding stimuli. Also, the localized surface plasmonic resonance (LSPR) of the superlattice monolayer film can be reversibly modulated by both by changing the local pH and applying an electric potential. Notably, a significant plasmonic shift of 157 nm can be achieved in the superlattice monolayer film when the PANI shell with a thickness of 35 nm and gold nanorods as a core were used. The superlattice monolayer film with dual-responsive plasmonic switches is promising for a range of potential applications in optoelectronic devices, plasmonic and colorimetric sensors, and surface-enhanced Raman scattering (SERS).

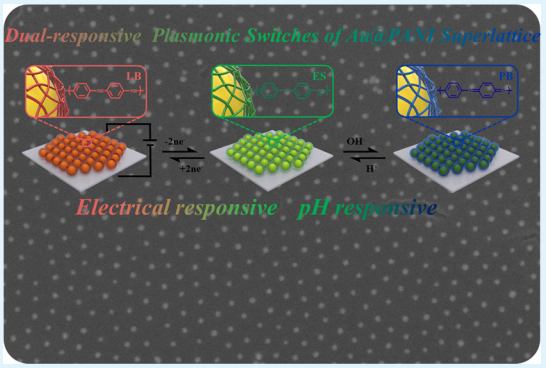

KEYWORDS: *core−shell structure, 2D monolayer film, superlattice, plasmonic switching, dual responsive*

1. INTRODUCTION

The self-assembly of inorganic nanoparticles (NPs) into a two-dimensional (2D) highly ordered array is of great significance in various fields such as electrical,[1,2] optical,[3,4] and magnetic devices.[5,6] Unlike the top-down methodologies including electron beam lithography (EBL),[7,8] photolithography,[9] and nanostencil lithography,[10] which typically require expensive equipments and are time-consuming, recently, bottom-up interfacial self-assembly has become an alternative strategy for constructing a 2D superlattice monolayer film that has large area and low cost and is easy to transfer.[11−13] Ordered nanoparticles arrays are primarily implemented with entropy-driven self-assembly strategies, such as by evaporation induction or destabilization.[14] It is worth noting that in the self-assembly process, the van der Waals (vdW) forces between the nanoparticles are particularly strong, especially between metal particles.[15] The effective method to resist vdW attraction is to provide steric hindrance by introducing soft ligands (molecules, DNA, polymers).[16] Therefore, embedding nanoparticle in the ligands is an effective and widely used approach to prevent excessive and disorderly packing. Using small-molecule ligands, the spacing of adjacent particles can be reduced to a small range of 1.2−2.3 nm,[17] which is of great importance for surface-enhanced Raman scattering (SERS).

It is important to point out that small-molecule ligands usually have a big challenge of inducing larger-sized nanoparticles for assembly into 2D or three-dimensional (3D) superlattices. These can be ascribed to the increase in the vdW

Received: February 2, 2020
Accepted: February 11, 2020
Published: February 11, 2020

https://dx.doi.org/10.1021/acsami.0c01983
ACS Appl. Mater. Interfaces 2020, 12, 11296−11304

attraction and the loss of active chain mobility on the surface of the NPs with the increase in the size of the NPs.[18] Such limitations could be effectively solved by introducing big molecules such as DNA or polymers, which often result in more spaces than that in small molecules. To date, a number of gold nanoparticle superlattices have been explored and the formed ordered arrays of nanoparticles have more distinctive collective properties than those of isolated nanoparticles or even disordered nanoparticle assemblies. For example, a nanoparticle superlattice can provide a coherent vibration mode[19] and increase p-type conductivity.[20] Superlattices of polymers and DNA-grafted nanoparticles show unusual mechanical properties[13] and distinctive plasmonic properties.[12]

To achieve a highly ordered arrangement of tunable optical responses, the gap between nanoparticles in traditional nanocrystal superlattices needs to be precisely controlled and greater than its coupling limit (more than 2.5 times the particle size).[21] It is also very important that the distance between the nanoparticles or the dielectric environment can be easily changed. Duan[22] et al. constructed amphiphilic gold nanoparticles by grafting polymers to form a 2D array with pH response at the oil−water interface. Cheng[12] et al. reported that PS-coated gold nanorods (Au NRs) by polymer-mediated interfacial self-assembly method were constructed into horizontal sheets (H-sheets) and vertical sheets (V-sheets) with different plasmonic properties, respectively. Mulvaney[23] et al. used the thermally responsive polymer (poly(*N*-isopropylacrylamide) (PNIPAM)) to graft the Au nanoparticles to construct a 2D superlattice film as an optical switch having a short response time and high reversibility can be realized. The reported responsive plasmonic systems usually had no superlattice structures, complex plasmonic mechanisms, or low plasmonic sensitivity, which limit their broader real-world applications.[24−26] Recently, free-standing, single-nanoparticle-thick plasmonic superlattice films have been introduced for a wide range of applications in microanalysis, sensor design, and optics.[27−30] However, due to the urgency of customizable new materials with tunable optical properties, the unique optical and electronic properties of nanoparticles are used to prepare self-assembled film with a macroscopically tunable optical superlattice array.

Herein, we report a method to use Au NPs@polyaniline (PANI) core/shell nanostructures for the self-assembly into a macroscopic 2D superlattice monolayer film at the oil−water interface. The PANI shell acts as a physical barrier to prevent attraction between the gold nanoparticles and prevent plasmonic coupling, which induces the orderly assembly of the gold nanoparticles as the shell thickness increases within a certain range. The pH and potential changes of the external environment cause the PANI shell to provide different dielectric environments, allowing the entire 2D superlattice monolayer to exhibit reversible plasmonic characterization and macroscopic color response.

2. METHODS

2.1. Materials. Chloroauric acid ($HAuCl_4 \cdot 3H_2O$, 99.9%) and cetrimonium bromide (CTAB) (>99.0%) were bought from Sigma-Aldrich. Trisodium citrate dehydrate (SC, ≥99.0%), tris-(hydroxymethyl)aminomethane (TB, GR), *n*-hexane (GR), sodium borohydride ($NaBH_4$, 99.0%), ascorbic acid (AA, 99.7%), silver nitrate ($AgNO_3$, >99.0%), and hydrochloric acid (HCl, 37 wt % in water) were purchased from Sinopharm Chemical Reagent Co., Ltd. (Shanghai). Sodium dodecyl sulfate (SDS, ACS, ≥99.0%), aniline (ACS, ≥99.0%), ammonium persulfate (AR, ≥98%), and ethanol absolute were obtained from Aladdin. All chemicals were used without further purification. Deionized water was used throughout the experiment process.

2.2. Characterization. UV−vis absorption spectra were recorded by a TU-1810 UV−vis spectrophotometer provided by Purkinje General Instrument Co., Ltd. Field-emission scanning electron microscopy (SEM) measurements were carried out using an S-4800 instrument (Hitachi) at an acceleration voltage of 8 kV. Transmission electron microscopy (TEM) was performed on a JEOL JEM-2100F electron microscope operating at 200 kV. Electrochemical measurements were performed on a CHI 660 electrochemical workstation (Chenhua Instrument Company, Shanghai, China).

2.3. Synthesis of Au NPs. Au NPs with a diameter of 35 nm were synthesized according to our reported method.[31,32] Briefly, SC (10 mL, 33 mM) was continuously added to boiling deionized water (140 mL) for 40 min. Then, fresh $HAuCl_4$ (1 mL, 25 mM) and TB solution (5 mL, 0.1 M) were sequentially added (time delay 60 s) with the temperature of the oil bath maintained at 137 °C. After 20 min, the temperature of the oil bath was reduced to 100 °C. Then, $HAuCl_4$ (1 mL, 25 mM) was injected twice into the solution at an interval of 20 min to improve the shape and size uniformity of the nanoparticles.

2.4. Synthesis of Au NRs. Synthesis of Au NRs was according to a previously reported method.[33−35]

2.5. Synthesis of Au NPs@PANI Core/Shell Nanostructures. The Au NPs@PANI core/shell nanostructures were prepared according to the previous method with some modifications.[36] The as-synthesized Au NPs (15 mL) were concentrated at 5500 g for 10 min to remove the supernatant. Then, the precipitate was redispersed in a mixture of aniline (2 μL) and SDS (2.5 mL, 40 mM). Then, the solution was shaken vigorously for 1 min. The resultant solution was mixed with an acidic $(NH4)_2S_2O_8$ solution (15 mL, 2 mM in 10 mM HCl) and further shaken for 30 s. Finally, the mixture was incubated at room temperature. The polymerization time can be changed to obtain a series of core/shell structures with different shell thicknesses. The PANI coating on the Au NRs followed the same procedure as the Au NPs with polymerization for 12 h.

2.6. Fabrication of Au NPs@PANI Core/Shell Superlattice Monolayer Film. The Au NPs@PANI core/shell nanostructure monolayer film was prepared according to our previous method with some modifications.[37] Briefly, the core/shell nanostructures (8 mL) and deionized water (3 mL) were added into a glass culture dish (6 cm in diameter), and hexane (10 mL) was slowly added to the surface of the aqueous solution to form an oil−water interface. Then, ethanol (10 mL) was injected into the aqueous solution at a uniform rate (0.4 mL/min). After the injection, the culture dish was covered with a glass slide to control the slow evaporation of hexane. The superlattice monolayer film was deposited on a transparent indium tin oxide (ITO) substrate and then immersed in water overnight to remove excessive SDS. Thereafter, it was immersed in a 0.1 M HCl solution for 1 h to obtain the doped emeraldine salt (ES) state of PANI.

2.7. Spectroelectrochemical Properties of Au NPs@PANI Superlattice Monolayer Film. The film on ITO was used as a working electrode, a platinum wire electrode as a counter electrode, and an Ag/AgCl (3 M KCl) electrode as a reference electrode. A solution of NaCl (0.5 M) in HCl (0.01 M) was used as an electrolyte. When an external voltage was applied to the film on the surface of the ITO, the color change of the film was observed in a very short time. However, we recorded the UV−vis spectra after applying the voltage for 20 s to ensure the entire conversion of the PANI shells. Spectroelectrochemical properties of Au NRs@PANI core/shell nanostructure monolayer film followed the same process as that for the superlattice monolayer film.

2.8. pH-Responsive Properties of Au NRs@PANI Core/Shell Monolayer Film. Monolayer film with Au NRs@PANI core/shell nanostructures was deposited on ITO placed into water whose pH was adjusted using NaOH (1 M) or HCl (1 M) solution. Similarly, we record the UV−vis spectra after dropping for 20 s to ensure the complete proton exchange of the PANI shells.

https://dx.doi.org/10.1021/acsami.0c01983
ACS Appl. Mater. Interfaces 2020, 12, 11296−11304

Scheme 1. (A) Schematic Illustrations of the Fabrication Process of Free-Standing Au NPs@PANI Superlattice Monolayer Film at the Air−Water Interface and (B) Monolayer Film Stimulated by pH or Potential and Chemical Structures of Resveratrol (LB), ES, and Pernigraniline Base (PB) States of PANI

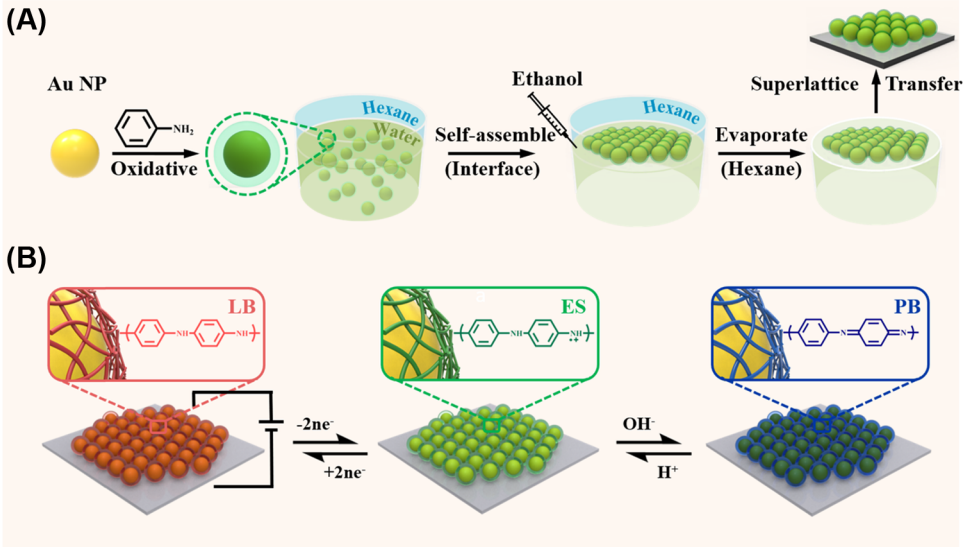

3. RESULTS AND DISCUSSION

3.1. Preparation Procedure of Au NPs@PANI Nanoparticle Superlattice Film. The preparation procedure and the principle of macroscopic Au NPs@PANI core/shell nanostructure superlattice monolayer film with dual-responsive plasmonic switches are shown in Scheme 1. The Au NPs@PANI core/shell nanostructures were realized through surfactant-assisted chemical oxidative polymerization of aniline in the presence of Au NPs. Then, Au NPs@PANI core/shell nanostructures self-assembled into a monolayer film at the oil−water interface. Using the optimized thickness of the PANI shell, the monolayer film can spontaneously form highly ordered structures (Scheme 1A). The optical color changed and reversible reactions of plasmonic properties were achieved by pH and potential stimulation (Scheme 1B).

3.2. Characterization of Au NPs@PANI Core/Shell Nanostructures. The transmission electron microscopy (TEM) images (Figure 1a,b) displayed Au NPs before and after the PANI coating. The average diameter of the Au NPs was 35 ± 3 nm. The Au NPs@PANI core/shell structures with different shell thicknesses (Figure 1c−h) were obtained by different times of polymerization. After two polymerization cycles, PANI with a shell thickness of 80 ± 10 nm was obtained (Figure S1). The UV−vis spectra of the Au NPs and the Au NPs@PANI core/shell nanostructures with different thicknesses of the PANI shell in aqueous solution were displayed in Figures 1i,j, S2, and S4. As the thickness of the PANI shell increased, the localized surface plasmonic resonance (LSPR) peak of the Au NPs@PANI core/shell nanostructures consistently red-shifted as well as the dispersion color changed from pink to brown (Figure 1j). According to previous reports,[32] polymerization time was used to adjust the core/shell nanostructures with different shell thicknesses.

3.3. Fabrication of Large-Area Au NP Monolayer Film. The monodisperse Au NPs were assembled into a large-area monolayer film at the water/n-hexane interface by injecting ethanol into the Au NPs solution. This method was utilized for self-assembly into a monolayer film over a large area; however, the assembled monolayer films were often accompanied by a large number of voids features due to the excess charge on the Au NPs surface.[37,38] In addition, due to the fixation of the transferred nanoparticles and the substrate, it was difficult to tune the plasmonic signature of the film by external conditions such as pH and voltage.[39] These disadvantages make it difficult to achieve the transfer of the 2D nano-monolayer film onto other substates for subsequent applications.

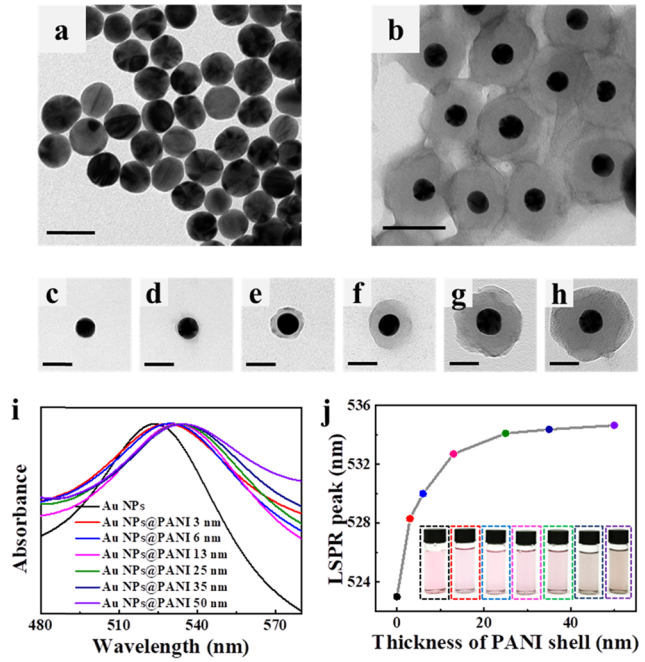

Figure 1. (a) TEM image of the uncoated Au NPs and (b) TEM image of Au NPs@PANI core/shell nanostructures with a shell thickness of 35 ± 3 nm. (c−h) TEM images of Au NPs@PANI core/shell nanostructures with different shell thicknesses. (i) Magnified UV−vis spectra of Au NPs and Au NPs@PANI core/shell nanostructures in aqueous solutions and (j) the optical photograph of the LSPR peak position of PANI to Au NPs as a function of the PANI shell thickness. The scale bars are (a−h) 50 nm.

https://dx.doi.org/10.1021/acsami.0c01983
ACS Appl. Mater. Interfaces 2020, 12, 11296−11304

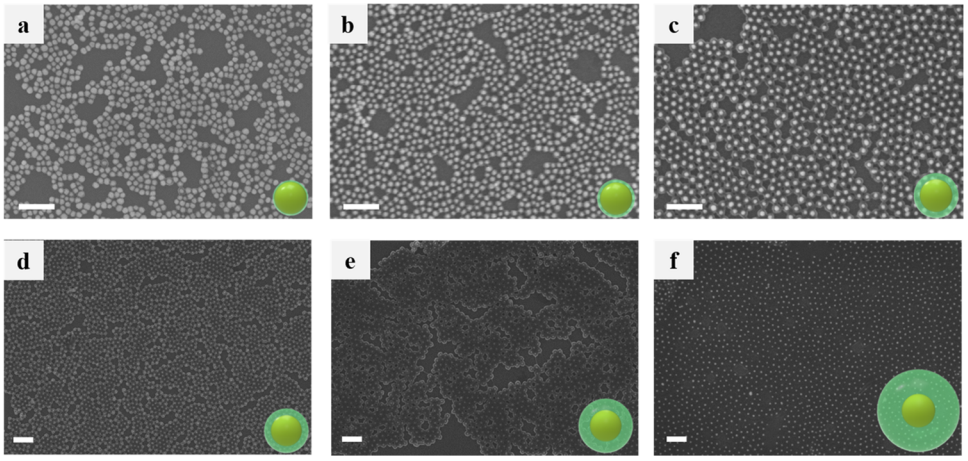

Figure 2. SEM images of interfacial Au NPs@PANI nanostructure monolayer films. (a–f) SEM images of Au NPs@PANI nanostructure monolayer films with different shell thicknesses. The scale bars are (a–c) 200 nm and (d–f) are 400 nm.

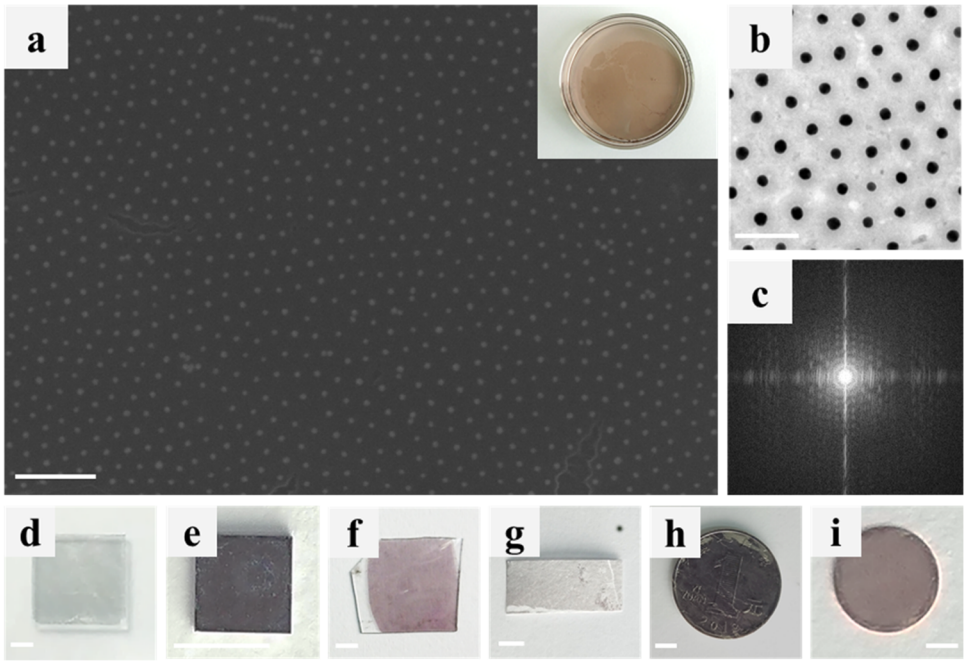

Figure 3. Au NPs@PANI core/shell nanostructures superlattice monolayer films. SEM image (a), TEM image (b), and fast Fourier transform (FFTs) of monolayer films (c) and the corresponding photographs (d–i) of Au NPs@PANI superlattice monolayer films transferred onto different substrates: ITO, silicon wafer, PDMS, filter paper, coin, and copper grid. The scale bars are (a) 500 nm, (b) 200 nm, (d–h) 0.5 cm, and (i) 0.1 cm.

The PANI shell as a stimuli-sensitive linker was coated on the surfaces of gold nanoparticles to obtain pH- and electrical-responsive properties, according to the previous report.[36] Then, the hexane was carefully injected onto the surface of the Au NP@PANI aqueous solution to form an incompatible oil–water interface. The nanostructures were trapped at the interface to form a monolayer film by uniformly adding ethanol to the aqueous solution. Mainly due to the competitive adsorption of ethanol, the surface charge was gradually reduced and the contact angle (less than 90°) of the hydrophilic nanoparticles tended to be 90°, the particles preferentially sank into the interface (Figure 2a–f).[40] Interestingly, the increase of the shell thickness leads to the gradually ordered arrangement of the nanostructures.

3.4. Fabrication of Large-Area Au NP Monolayer Superlattice Film. It is well known that the steric hindrance of polymer ligand–ligand can generally counteract the vdW attraction between adjacent NPs, enabling superlattice self-assembly.[16] The particle orientation of the final superlattice can be determined by manipulating the chain length of the polymer to control the interaction between the nanoparticles.[41] It was also reported[42] that short ligands would lead to the formation of cracks and multilayered disordered structures. The assembled structures exhibited a disordered and loose structure when long ligands are used. These orientations can be explained by the interaction forces based on the nanoscale between the particles during assembly. The steric hindrance brought by the long ligand outweighs the vdW forces, and the short ligand makes the steric hindrance dominant. NPs with a thin PANI shell (3–13 nm) were distributed at the oil–water interface. It was easy to find that NPs formed island-like clusters during the self-assembly (Figure 2a–c). As the shell thickness increases further (25–35 nm), the arrangement gradually tends to become ordered (Figure 2d,e). When the

https://dx.doi.org/10.1021/acsami.0c01983
ACS Appl. Mater. Interfaces 2020, 12, 11296–11304

thickness of the PANI shell is increased to about 50 nm, a superlattice monolayer film was obtained (Figure 2f). After two polymerization cycles, the superlattice array feature in the film of the Au NPs@PANI nanostructures with a thick (80 ± 10 nm) PANI shell (Figure S2) was disappeared (Figure S3). It is suspected that the inhomogeneity can be ascribed to the broad particle size distribution of the nanostructures and electrostatic repulsion against long-range vdW interaction.[36,39]

According to the oil−water interfacial self-assembly method, a large area of 2D superlattice monolayer film (centimeter scale) can be fabricated by selecting the appropriate PANI shell thickness and particle core size (Figure 3a). A fast Fourier transform (FFT) analysis of the respective electron micrograph with well-defined spots indicated a high degree of order with Au NPs@PANI (Figure 3b,c), which was similar to other superlattice-related reports.[13] Simultaneously, the transferability of the superlattice film was verified; so, it can be transferred to various substrates, such as ITO, silicon wafer, poly(dimethylsiloxane) (PDMS), filter paper, coin, and copper grid (shown in Figure 3d−i) to develop subsequent functional devices.[43]

3.5. Dual-Responsive Plasmonic Behavior. In the environment of different pH values and redox states, PANI can exist in three states: emeraldine salt (ES), resveratrol (LB), and pernigraniline base (PB).[44] Each state has a different refractive index. By adding acid or base, PANI can exist in the ES or PB state by doping and dedoping of protons. It should be noted that the absorption peak position of Au NPs was too close to the peak position of PB, which made it difficult to determine the specific plasmonic peak shift. It has been reported that through electrochemical control in the aqueous or nonaqueous phase, the ES state of PANI shells can be reversibly transformed into the LB state. The superlattice monolayer film was transferred onto the ITO substrate. Considering the redox of PANI and avoiding damage to ITO.[45] The selection voltage range was −0.3 to 0.5 V. The slightly acid brine solution (0.5 M NaCl in 0.01 M HCl) could obtain a greater plasmonic peak shift.[46] The deposited ITO of the superlattice monolayer film was immersed in aqueous hydrochloric acid for 6 h to ensure that all PANI shells were converted to the ES states. The real-time observation of the spectral changes of the Au NPs@PANI core/shell nanostructure monolayer film under the electrochemical switching was achieved using a custom-designed electrochemical cell, as schematically shown in Figure S10. In Figure 4a, the UV−vis spectra are displayed at different voltages in the electrolyte. From the voltage of −0.3 to 0 V, the position of the plasmonic peak did not change much because of the characteristics of the LB state. The mutation point started at 0 V, and the absorbance around 800 nm began to increase. These phenomena indicated that the LB state began to convert to ES. Overall, from −0.3 to 0.5 V, the position of the LSPR was approximately 12 nm (from 548 to 536 nm; Figures 4a,b and S5). Plasmonic responsiveness of the superlattice monolayer film can be explained using the mechanism as illustrated in Figure 4e. After 10 voltage cycles, we found that the position of the LSPR remains stable, indicating that the reversible stability of the superlattice film for voltage-controlled plasmonic peak shifts (Figure 4c). The response time of the PANI shell state transition at a constant voltage can be seen from the current curve in Figure S6. To further verify the stability of the monolayer film, 100 cyclic voltammetry (CV) cycles were tested within the range from −0.3 to 0.5 V (vs Ag/AgCl) at

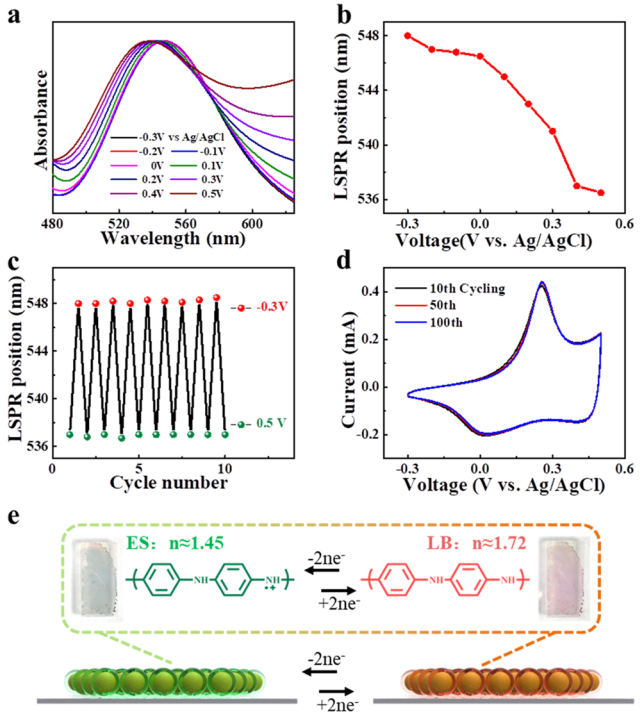

Figure 4. Plasmonic switching behavior and proposed mechanism of the Au NPs@PANI nanostructure superlattice monolayer film. (a) Magnified UV−vis spectra of Au NPs@PANI core/shell nanostructure superlattice monolayer film with a shell thickness of 50 ± 5 nm at different voltages with 0.5 M NaCl in 0.01 M HCl electrolyte and (b) their LSPR peak position vs voltages (Ag/AgCl). (c) LSPR peak position during cycling at −0.3 and 0.5 V. (d) Cyclic voltammograms (CV) of Au NPs@PANI core/shell nanostructure superlattice of monolayer film with a shell thickness of 50 ± 5 nm at 100 mV/s from −0.3 to 0.5 V during cycling. (e) Proposed mechanism for plasmonic switching of Au NPs@PANI superlattice monolayer film from −0.3 to 0.5 V.

100 mV/s. The CV measurement (Figure 4d) showed no significant decrease in electroactivity in the curve after 100 cycles, demonstrating the electrochemical stability of the superlattice film.

To achieve a double responsive signal, the Au NPs were replaced with Au NRs. Figures 5a,b and S7 displayed SEM images of the Au NR monolayer film before and after PANI coating. The average length and diameter of the Au NRs were 100 ± 7 and 48 ± 5 nm, respectively. The average thicknesses of the PANI shells on Au NRs were 35 ± 5 nm. The UV−vis spectra of the Au NRs before and after PANI coating in aqueous solution are shown in Figure 5c. The bare Au NRs displayed an ensemble longitudinal plasmon resonance wavelength of 685 nm in aqueous solution. The conductive ES form peak of PANI is located at around 800 nm in acid aqueous condition. When the pH was adjusted to 11, PANI was changed from the ES to the PB form, and the peak around 800 nm was shifted to about 560 nm, which was the characteristic of the PB form (Figure 5d).[47]

Obviously, the longitudinal plasmon peak of the Au NRs showed a huge red-shift from 665 to 822 nm (Figure 5c), as PB has a much bigger refractive index than ES.[46] In our system, the longitudinal plasmon peak of the Au NRs was mainly investigated because the apparent red-shift (157 nm), and the transverse plasmon peak was too close to the characteristic peak of the PB to form a broad peak.

https://dx.doi.org/10.1021/acsami.0c01983
ACS Appl. Mater. Interfaces 2020, 12, 11296−11304

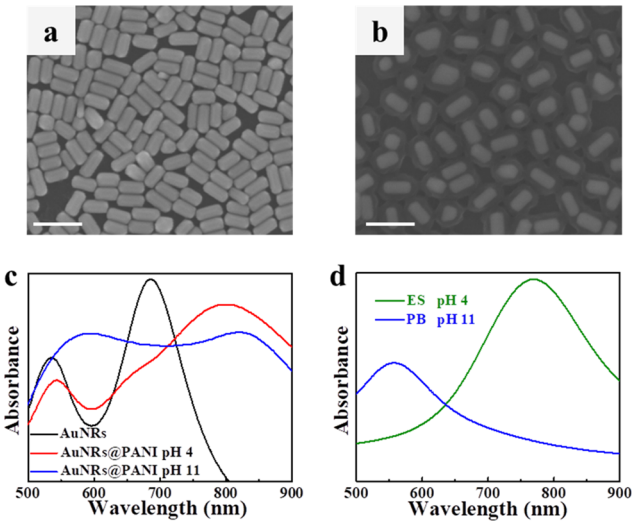

Figure 5. Au NRs and Au NRs@PANI structures and monolayer film. (a) SEM images of Au NR monolayer film and (b) SEM image of Au NRs@PANI nanostructure monolayer film. (c) Magnified UV−vis spectra of Au NRs@PANI core/shell nanostructure monolayer film with a shell thickness of 35 ± 5 nm at environmental pH 4 and 11. (d) UV−vis spectra of ES and PB form of PANI. The scale bars are (a, b) 100 nm.

To test the pH and electrical behavior, the Au NRs@PANI core/shell nanostructure monolayer film was transferred onto the ITO substrate. The Au NRs@PANI core/shell nanostructure monolayer film on ITO had the pH response behavior similar to that of Au NRs@PANI core/shell nanostructures in aqueous solution (Figures 5c, 6a, and S8). When the pH of the solution was 2, three peaks showed at 552, 665, and 831 nm, arising from the transverse, longitudinal plasmon peak of Au NRs, and the absorption of ES form, respectively. When the pH was further increased, the peak intensity at around 830 nm began to decrease and the peak at 665 nm was red-shifted to 820 nm until the pH was 11. These results indicated that the PANI shells converted from doped ES form to undoped PB form. At the same time, the extinction peak position was nearly completely reversible, while the pH was repeatedly varied between 2 and 11 (Figure 6b). The electrical response test of Au NRs@PANI nanostructures monolayer film was performed according to the previous method.[44,47] PANI can be converted from ES form to LB form by voltage regulation. The UV−vis spectra of the film at different voltages are shown in Figures 6d and S9. At a low potential (−0.3 V), PANI was in the form of LB and the absorbance peak of the Au NRs was located at 754 nm. As the voltage increased, the position of the UV peak continuously blue-shifted to 660 nm, indicating that PANI was restored to the ES form. The nearly completely reversible oscillation of the extinction peak position was also observed during the 10-cycle voltage switching (Figure 6e). Plasmonic responsiveness of the Au NRs@PANI core/shell nanostructure monolayer film can be explained using the mechanism as illustrated in Figure 6c,f. Comparing the electrical property with the pH response, the pH response gave the largest plasma peak shift of the monolayer film because the refractive index of PB was higher than that of ES or LB.[48]

3.6. Formation Mechanism of Superlattices. PANI was used as a soft ligand shell to cover the nanoparticles and implemented a superlattice arrangement through a bottom-up self-assembly strategy. The typical roles of PANI soft ligand shell in the process of self-assembly mainly includes four parts. (a) The introduction of a shell layer of appropriate thickness as a physical spacer could offset the van der Waals (vdW) and electrostatic forces of a steric hindrance to prevent the disordered aggregation of inorganic nanoparticles. (b) The nanoforce is adjusted to adjust the potential between particles. (c) The overall mechanical integrity of the superlattice is maintained through strong ligand interactions. (d) The electrochemical activity of the PANI layer can be used for the tunable dielectric environment of the superlattice film.[16,49]

In the process of constructing an energy well of the oil−water interface to obtain a 2D monolayer film, the film is often breakable and disordered due to the weak physical interaction

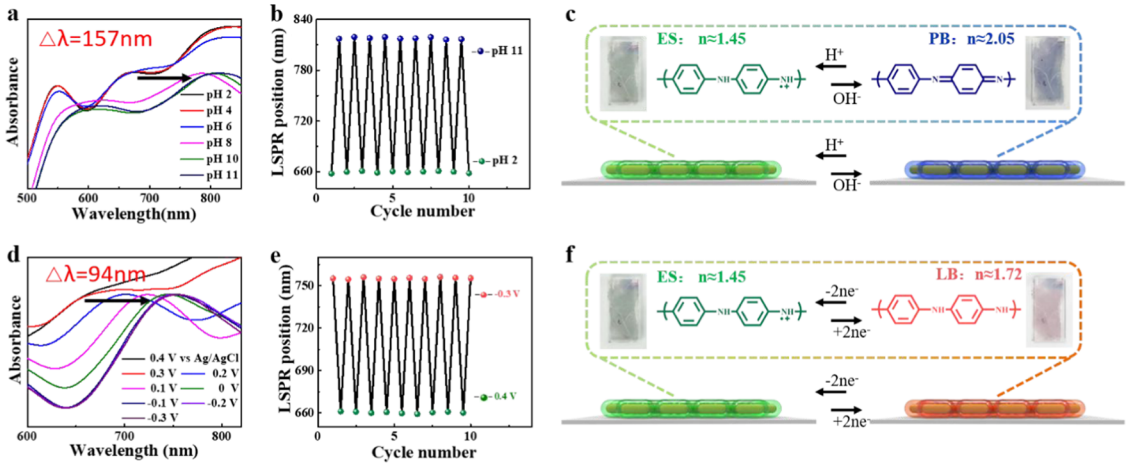

Figure 6. Plasmonic switching behavior and proposed mechanisms of the Au NRs@PANI nanostructure monolayer films. (a) Magnified UV−vis spectra of Au NRs@PANI core/shell nanostructure monolayer film with a shell thickness of 35 ± 5 nm at different environmental pH and its (b) LSPR peak position upon pH change during cycling. (c) Proposed mechanism of the plasmonic switching of Au NRs@PANI core/shell nanostructures monolayer film by adding acid or base. (d) Magnified UV−vis spectra of Au NRs@PANI core/shell nanostructure monolayer film with a shell thickness of 35 ± 5 nm at different voltages with 0.5 M NaCl in 0.01 M HCl electrolyte and its (e) LSPR peak position upon electrical potential change during cycling. (f) Proposed mechanism for plasmonic switching of Au NRs@PANI core/shell nanostructures monolayer film at different electrical potentials.

https://dx.doi.org/10.1021/acsami.0c01983
ACS Appl. Mater. Interfaces 2020, 12, 11296−11304

between the particles and the volatilization of *n*-hexane as a protective layer.[37] When a soft ligand is coated around the nanoparticles, the gap formed by the assembly of spherical particles can be filled by forming a 2D film that is single-nanoparticle thick. Through the continuous injection of ethanol to squeeze the nanoparticles to form a more robust physical entanglement and the interaction of chemical ligands form an ordered arrangement of the superlattice, which keeps the integrity of the superlattice 2D film during the volatilization of *n*-hexane.[50]

The potential for the interaction of soft spheres actually contributes to the vdW forces between the hard core and spatial exclusion of soft ligands (Figure 7). Fitzmaurice

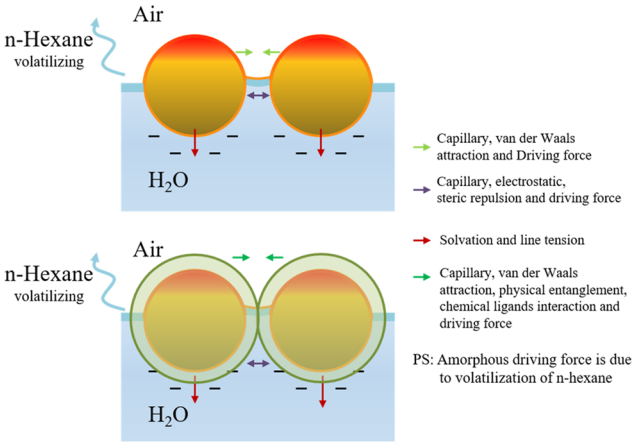

Figure 7. Force changes between nanoparticles before and after the modification of soft ligands on the surface of particles.

proposed a soft sphere model to show that the total interaction potential (U_{total}) between particles can be quantitatively estimated as the contribution of vdW attraction potential (U_{vdW}) and spatial exclusion potential (U_{steric})[51]

$$U_{total} = U_{vdW} + U_{steric}$$

Simultaneously, some studies also have shown that the length of the polymer ligand was also a key factor that directly affects the stacking order and quality of the 2D superlattice film.[41,42] To form an ordered array, the vdW attractive force needs to be balanced with the steric hindrance of the soft ligand. For longer ligands, the steric force was likely to dominate, while for shorter ligands, the vdW force outweighs the steric resistance. An ordered superlattice cannot be obtained in either case.

To expand the application, 2D superlattice monolayer films were successfully used to prepare intelligent color-changing windows. As shown in Figure 8, the color of the 2D film changed through the adjustment of pH and voltage. This phenomenon is caused by the doped state ES and the undoped

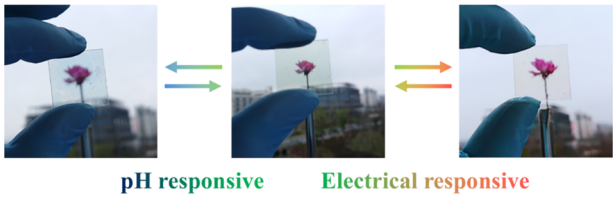

Figure 8. Color response of 2D superlattice monolayer films at different pH values and voltages.

state PB shells, which can absorb light to reflect green and violet colors. However, the voltage-stimulated LB state is transparent under visible light, which means that more light reaches the gold nanoparticles and the original red-wine color of gold nanoparticles is shown. Figure S6 shows the fast electrical switching speed of our intelligent color-changing window, about 3 s, which reflected the certain application potential of the 2D self-supporting film for optical devices.

3.7. Mechanism of the Electromagnetically Responsive Plasmonic Resonance. The state of the PANI shell can be changed by changing the pH value and the voltage of the external environment, thereby changing the dielectric environment around the gold nanoparticles. Interestingly, while the nanoparticles were assembled into a 2D film, the PANI shell acted as a physical spacer while preventing plasma coupling between the particles or the substrate. This special electroactive medium was used to solve the plasmonic coupling and give the tunable plasmonic properties of the whole 2D film.

The LSPR shift of plasmonic nanoparticles has been found to follow the following relationship

$$\Delta\lambda_{shift} = m\Delta n(1 - e^{-2d/l_d})$$

where m is the refractive index sensitivity of the plasmonic nanoparticles, Δn is the change in refractive indexes between the shell types at the plasmon resonance of the nanoparticles, d is the effective thickness of the dielectric adsorbate layer, and l_d is the decay length of the electromagnetic field at the plasmonic nanoparticle surface, respectively.[52]

For nanoparticles of given dielectric layer thickness, $\Delta\lambda_{shift}$ depends on the difference in the dielectric environment change. The refractive index measurements of PANI with ES, PB, and LB were according to previous work. In an acid−base environment, the difference between the doped state ES and the undoped state PB was greater than the difference between the ES and LB states when the voltage was switched. The experimental results using Au NR@PANI also supported this theory (157 > 94 nm). It is believed that nanoparticles with high plasmonic sensitivity, such as gold nanopyramids, may result in a stronger plasmonic shift for various applications.[53]

4. CONCLUSIONS

In summary, we demonstrated a simple and robust interfacial self-assembly method to fabricate the stimuli-responsive large-area superlattice monolayer at the oil−water interface. The Au NPs@PANI core/shell superlattice monolayer film can be easily transferred onto substrates such as conductive ITO and silicon wafers. The appropriate thickness of the PANI shell not only induced nanoparticle directional assembly but also avoided unwanted plasmonic resonance coupling as a physical separation. Notably, a significant plasmonic shift of monolayer film can be achieved at 157 nm, when 35 nm thick PANI shell and gold nanorods as core were used. The superlattice monolayer film with dual-responsive plasmonic switches is promising for a range of potential applications in optoelectronic devices, plasmonic and colorimetric sensors, and surface-enhanced Raman scattering (SERS).

■ ASSOCIATED CONTENT

Supporting Information

The Supporting Information is available free of charge at https://pubs.acs.org/doi/10.1021/acsami.0c01983.

https://dx.doi.org/10.1021/acsami.0c01983
ACS Appl. Mater. Interfaces 2020, 12, 11296−11304

TEM image and UV−vis spectra of Au NPs@PANI core/shell nanostructures obtained at different polymerization times, SEM image of Au NPs@PANI core/shell nanostructure monolayer film, UV−vis spectra of a superlattice monolayer film at different voltages, amperometric i−t curve of the Au NPs@PANI core/shell nanostructure superlattice monolayer film, and the three-electrode electrochemical cell for the real-time measurements of the extinction spectra (PDF)

AUTHOR INFORMATION

Corresponding Authors

Youju Huang − *College of Materials, Chemistry and Chemical Engineering, Hangzhou Normal University, Hangzhou, Zhejiang 311121, P. R. China; Key Laboratory of Marine Materials and Related Technologies, Zhejiang Key Laboratory of Marine Materials and Protective Technologies, Ningbo Institute of Materials Technology and Engineering, Chinese Academy of Sciences, Ningbo 315201, China;* orcid.org/0000-0001-5815-9784; Email: yjhuang@hznu.edu.cn

Zhiyong Guo − *China State Key Laboratory for Quality and Safety of Agro-products, State Key Laboratory Base of Novel Functional Materials and Preparation Science, School of Materials Science and Chemical Engineering, Ningbo University, Ningbo 315211, P. R. China;* orcid.org/0000-0003-1288-1573; Email: guozhiyong@nbu.edu.cn

Tao Chen − *Key Laboratory of Marine Materials and Related Technologies, Zhejiang Key Laboratory of Marine Materials and Protective Technologies, Ningbo Institute of Materials Technology and Engineering, Chinese Academy of Sciences, Ningbo 315201, China;* orcid.org/0000-0001-9704-9545; Email: tao.chen@nimte.ac.cn

Authors

Han Lin − *College of Materials, Chemistry and Chemical Engineering, Hangzhou Normal University, Hangzhou, Zhejiang 311121, P. R. China; China State Key Laboratory for Quality and Safety of Agro-products, State Key Laboratory Base of Novel Functional Materials and Preparation Science, School of Materials Science and Chemical Engineering, Ningbo University, Ningbo 315211, P. R. China*

Liping Song − *Key Laboratory of Marine Materials and Related Technologies, Zhejiang Key Laboratory of Marine Materials and Protective Technologies, Ningbo Institute of Materials Technology and Engineering, Chinese Academy of Sciences, Ningbo 315201, China*

Qian Cheng − *Key Laboratory of Marine Materials and Related Technologies, Zhejiang Key Laboratory of Marine Materials and Protective Technologies, Ningbo Institute of Materials Technology and Engineering, Chinese Academy of Sciences, Ningbo 315201, China*

Yanping Yang − *Key Laboratory of Marine Materials and Related Technologies, Zhejiang Key Laboratory of Marine Materials and Protective Technologies, Ningbo Institute of Materials Technology and Engineering, Chinese Academy of Sciences, Ningbo 315201, China*

Fengmei Su − *National Engineering Research Centre for Advanced Polymer Processing Technology, Key Laboratory of Materials Processing and Mold (Zhengzhou University), Ministry of Education, Zhengzhou University, Zhengzhou 450002, P. R. China*

Complete contact information is available at: https://pubs.acs.org/10.1021/acsami.0c01983

Notes

The authors declare no competing financial interest.

ACKNOWLEDGMENTS

The authors gratefully acknowledge the National Natural Science Foundation of China (grant nos. 51873222 and 81773483), the State Key Laboratory for Managing Biotic and Chemical Threats to the Quality and Safety of Agro-products (ZS20190101 and KF20190101), the Fujian Province-Chinese Academy of Sciences STS project (2017T31010024), Key Research Program of Frontier Science, Chinese Academy of Sciences (QYZDB-SSW-SLH036), and the Ningbo Science and Technology Bureau (2019A610204). This work was also sponsored by the start-up funding from Hangzhou Normal University and K. C. Wong Magna Fund in Ningbo University.

REFERENCES

(1) Parthasarathy, R.; Lin, X.-M.; Jaeger, H. M. Electronic Transport in Metal Nanocrystal Arrays: The Effect of Structural Disorder on Scaling Behavior. *Phys. Rev. Lett.* **2001**, *87*, No. 186807.

(2) Kim, S.-H.; Medeiros-Ribeiro, G.; Ohlberg, D. A. A.; Williams, R. S.; Heath, J. R. Individual and Collective Electronic Properties of Ag Nanocrystals. *J. Phys. Chem. B* **1999**, *103*, 10341−10347.

(3) Kagan, C. R.; Murray, C. B.; Nirmal, M.; Bawendi, M. G. Electronic Energy Transfer in CdSe Quantum Dot Solids. *Phys. Rev. Lett.* **1996**, *76*, 1517−1520.

(4) Collier, C. P.; Saykally, R. J.; Shiang, J. J.; Henrichs, S. E.; Heath, J. R. Reversible Tuning of Silver Quantum Dot Monolayers Through the Metal-Insulator Transition. *Science* **1997**, *277*, 1978−1981.

(5) de Jonge, N.; Lamy, Y.; Schoots, K.; Oosterkamp, T. H. High brightness electron beam from a multi-walled carbon nanotube. *Nature* **2002**, *420*, 393−395.

(6) Murray, C. B.; Sun, S. H.; Gaschler, W.; Doyle, H.; Betley, T. A.; Kagan, C. R. Colloidal synthesis of nanocrystals and nanocrystal superlattices. *IBM J. Res. Dev.* **2001**, *45*, 47−56.

(7) Wang, L.; Xiong, W.; Nishijima, Y.; Yokota, Y.; Ueno, K.; Misawa, H.; Qiu, J.; Bi, G. Spectral properties of nanoengineered Ag Au bilayerrods fabricated by electron beam lithography. *Appl. Opt.* **2011**, *50*, 5600−5605.

(8) Ueno, K.; Misawa, H. Spectral properties and electromagnetic field enhancement effects on nano-engineered metallic nanoparticles. *Phys. Chem. Chem. Phys.* **2013**, *15*, 4093−4099.

(9) Bowen, A. M.; Nuzzo, R. G. Fabrication of Flexible Binary Amplitude Masks for Patterning on Highly Curved Surfaces. *Adv. Funct. Mater.* **2009**, *19*, 3243−3253.

(10) Aksu, S.; Huang, M.; Artar, A.; Yanik, A. A.; Selvarasah, S.; Dokmeci, M. R.; Altug, H. Flexible plasmonics on unconventional and nonplanar substrates. *Adv. Mater.* **2011**, *23*, 4422−4430.

(11) Cheng, W.; Park, N.; Walter, M. T.; Hartman, M. R.; Luo, D. Nanopatterning self-assembled nanoparticle superlattices by moulding microdroplets. *Nat. Nanotechnol.* **2008**, *3*, 682−690.

(12) Ng, K. C.; Udagedara, I. B.; Rukhlenko, I. D.; Chen, Y.; Tang, Y.; Premaratne, M.; Cheng, W. Free-Standing Plasmonic-Nanorod Superlattice Sheets. *ACS Nano* **2012**, *6*, 925−934.

(13) Cheng, W.; Campolongo, M. J.; Cha, J. J.; Tan, S. J.; Umbach, C. C.; Muller, D. A.; Luo, D. Free-standing nanoparticle superlattice sheets controlled by DNA. *Nat. Mater.* **2009**, *8*, 519−525.

(14) Murray, C. B.; Kagan, C. R.; Bawendi, M. G. Self-organization of CdSe Nanocrystallites intoThree-Dimensional Quantum Dot Superlattices. *Science* **1995**, *270*, 1335−1338.

(15) Bishop, K. J.; Wilmer, C. E.; Soh, S.; Grzybowski, B. A. Nanoscale forces and their uses in self-assembly. *Small* **2009**, *5*, 1600−1630.

(16) Si, K. J.; Chen, Y.; Shi, Q.; Cheng, W. Nanoparticle Superlattices: The Roles of Soft Ligands. *Adv. Sci.* **2018**, *5*, No. 1700179.
(17) Martin, J. E.; Wilcoxon, J. P.; Odinek, J.; Provencio, P. Control of the Interparticle Spacing in Gold Nanoparticle Superlattices. *J. Phys. Chem. B* **2000**, *104*, 9475−9486.
(18) Kim, B.; Tripp, S. L.; Wei, A. Self-Organization of Large Gold Nanoparticle Arrays. *J. Am. Chem. Soc.* **2001**, *123*, 7955−7956.
(19) Courty, A.; Mermet, A.; Albouy, P. A.; Duval, E.; Pileni, M. P. Vibrational coherence of self-organized silver nanocrystals in f.c.c. supra-crystals. *Nat. Mater.* **2005**, *4*, 395−398.
(20) Urban, J. J.; Talapin, D. V.; Shevchenko, E. V.; Kagan, C. R.; Murray, C. B. Synergism in binary nanocrystal superlattices leads to enhanced p-type conductivity in self-assembled PbTe/Ag2 Te thin films. *Nat. Mater.* **2007**, *6*, 115−121.
(21) Su, K.-H.; Wei, Q.-H.; Zhang, X.; Mock, J. J.; Smith, D. R.; Schultz, S. Interparticle Coupling Effects on Plasmon Resonances of Nanogold Particles. *Nano Lett.* **2003**, *3*, 1087−1090.
(22) Cheng, L.; Liu, A.; Peng, S.; Duan, H. Responsive Plasmonic Assemblies of Amphiphilic Nanocrystals at Oil-Water Interfaces. *ACS Nano* **2010**, *4*, 6098−6104.
(23) Karg, M.; Hellweg, T.; Mulvaney, P. Self-Assembly of Tunable Nanocrystal Superlattices Using Poly-(NIPAM) Spacers. *Adv. Funct. Mater.* **2011**, *21*, 4668−4676.
(24) Lv, W.; Liu, S.; Fan, X.; Wang, S.; Zhang, G.; Zhang, F. Gold Nanoparticles Functionalized by a Dextran-Based pH- and Temperature-Sensitive Polymer. *Macromol. Rapid Commun.* **2010**, *31*, 454−458.
(25) Strozyk, M. S.; Chanana, M.; Pastoriza-Santos, I.; Pérez-Juste, J.; Liz-Marzán, L. M. Protein/Polymer-Based Dual-Responsive Gold Nanoparticles with pH-Dependent Thermal Sensitivity. *Adv. Funct. Mater.* **2012**, *22*, 1436−1444.
(26) Song, L.; Sun, H.; Chen, X.; Han, X.; Liu, H. From multi-responsive tri- and diblock copolymers to diblock-copolymer-decorated gold nanoparticles: the effect of architecture on micellization behaviors in aqueous solutions. *Soft Matter* **2015**, *11*, 4830−4839.
(27) Hellweg, T. Towards large-scale photonic crystals with tuneable bandgaps. *Angew. Chem., Int. Ed.* **2009**, *48*, 6777−6778.
(28) Joannopoulos, J. D.; Villeneuve, P. R.; Fan, S. Photonic crystals: putting a new twist on light. *Nature* **1997**, *386*, 143−149.
(29) Chen, L.; Huang, Y.; Song, L.; Yin, W.; Hou, L.; Liu, X.; Chen, T. Biofriendly and Regenerable Emotional Monitor from Interfacial Ultrathin 2D PDA/AuNPs Cross-linking Films. *ACS Appl. Mater. Interfaces* **2019**, *11*, 36259−36269.
(30) Kannan, P.; Chen, J.; Su, F.; Guo, Z.; Huang, Y. Faraday-Cage-Type Electrochemiluminescence Immunoassay: A Rise of Advanced Biosensing Strategy. *Anal. Chem.* **2019**, *91*, 14792−14802.
(31) Lu, X.; Dandapat, A.; Huang, Y.; Zhang, L.; Rong, Y.; Dai, L.; Sasson, Y.; Zhang, J.; Chen, T. Tris base assisted synthesis of monodispersed citrate-capped gold nanospheres with tunable size. *RSC Adv.* **2016**, *6*, 60916−60921.
(32) Cheng, Q.; Song, L.; Lin, H.; Yang, Y.; Huang, Y.; Su, F.; Chen, T. Free-Standing 2D Janus Gold Nanoparticles Monolayer Film with Tunable Bifacial Morphologies via the Asymmetric Growth at Air-Liquid Interface. *Langmuir* **2020**, *36*, 250−256.
(33) Ye, X.; Zheng, C.; Chen, J.; Gao, Y.; Murray, C. B. Using binary surfactant mixtures to simultaneously improve the dimensional tunability and monodispersity in the seeded growth of gold nanorods. *Nano Lett.* **2013**, *13*, 765−771.
(34) Dai, L.; Song, L.; Huang, Y.; Zhang, L.; Lu, X.; Zhang, J.; Chen, T. Bimetallic Au Ag Core-Shell Superstructures with Tunable Surface Plasmon Resonance in the Near-Infrared Region and High Performance Surface-Enhanced Raman Scattering. *Langmuir* **2017**, *33*, 5378−5384.
(35) Yang, Y.; Song, L.; Huang, Y.; Chen, K.; Cheng, Q.; Lin, H.; Xiao, P.; Liang, Y.; Qiang, M.; Su, F.; Chen, T. Asymmetrical Molecular Decoration of Gold Nanorods for Engineering of Shape-Controlled AuNR@Ag Core-Shell Nanostructures. *Langmuir* **2019**, *35*, 16900−16906.
(36) Xing, S.; Tan, L. H.; Yang, M.; Pan, M.; Lv, Y.; Tang, Q.; Yang, Y.; Chen, H. Highly controlled core shell structures tunable conductive polymer shells on gold nanoparticles and nanochains. *J. Mater. Chem.* **2009**, *19*, 3286−3291.
(37) Lu, X.; Huang, Y.; Liu, B.; Zhang, L.; Song, L.; Zhang, J.; Zhang, A.; Chen, T. Light-Controlled Shrinkage of Large-Area Gold Nanoparticle Monolayer Film for Tunable SERS Activity. *Chem. Mater.* **2018**, *30*, 1989−1997.
(38) Hu, L.; Chen, M.; Fang, X.; Wu, L. Oil-water interfacial self-assembly: a novel strategy for nanofilm and nanodevice fabrication. *Chem. Soc. Rev.* **2012**, *41*, 1350−1362.
(39) Liu, B.; Lu, X.; Qiao, Z.; Song, L.; Cheng, Q.; Zhang, J.; Zhang, A.; Huang, Y.; Chen, T. pH and Temperature Dual-Responsive Plasmonic Switches of Gold Nanoparticle Monolayer Film for Multiple Anticounterfeiting. *Langmuir* **2018**, *34*, 13047−13056.
(40) Duan, H.; Wang, D.; Kurth, D. G.; Mohwald, H. Directing self-assembly of nanoparticles at water oil interfaces. *Angew. Chem.* **2004**, *116*, 5757−5760.
(41) Yun, H.; Yu, J. W.; Lee, Y. J.; Kim, J. S.; Park, C. H.; Nam, C.; Han, J.; Heo, T. Y.; Choi, S.-H.; Lee, D. C.; Lee, W. B.; Stein, G. E.; Kim, B. J. Symmetry Transitions of Polymer-Grafted Nanoparticles Grafting Density Effect. *Chem. Mater.* **2019**, *31*, 5264−5273.
(42) Shi, Q.; Si, K. J.; Sikdar, D.; Yap, L. W.; Premaratne, M.; Cheng, W. Two-Dimensional Bipyramid Plasmonic Nanoparticle Liquid Crystalline Superstructure with Four Distinct Orientational Packing Orders. *ACS Nano* **2016**, *10*, 967−976.
(43) Reincke, F.; Hickey, S. G.; Kegel, W. K.; Vanmaekelbergh, D. Spontaneous assembly of a monolayer of charged gold nanocrystals at the water/oil interface. *Angew. Chem., Int. Ed.* **2004**, *43*, 458−462.
(44) Jeon, J. W.; Ma, Y.; Mike, J. F.; Shao, L.; Balbuena, P. B.; Lutkenhaus, J. L. Oxidatively stable polyaniline:polyacid electrodes for electrochemical energy storage. *Phys. Chem. Chem. Phys.* **2013**, *15*, 9654−9662.
(45) Lu, W.; Jiang, N.; Wang, J. Active Electrochemical Plasmonic Switching on Polyaniline-Coated Gold Nanocrystals. *Adv. Mater.* **2017**, *29*, No. 1604862.
(46) Jeon, J. W.; Ledin, P. A.; Geldmeier, J. A.; Ponder, J. F.; Mahmoud, M. A.; El-Sayed, M.; Reynolds, J. R.; Tsukruk, V. V. Electrically Controlled Plasmonic Behavior of Gold Nanocube@ Polyaniline Nanostructures Transparent Plasmonic Aggregates. *Chem. Mater.* **2016**, *28*, 2868−2881.
(47) Jiang, N.; Shao, L.; Wang, J. (Gold nanorod core)/(polyaniline shell) plasmonic switches with large plasmon shifts and modulation depths. *Adv. Mater.* **2014**, *26*, 3282−3289.
(48) Jeon, J. W.; Zhou, J.; Geldmeier, J. A.; Ponder, J. F.; Mahmoud, M. A.; El-Sayed, M.; Reynolds, J. R.; Tsukruk, V. V. Dual-Responsive Reversible Plasmonic Behavior of Core−Shell Nanostructures with pH-Sensitive and Electroactive Polymer Shells. *Chem. Mater.* **2016**, *28*, 7551−7563.
(49) Yi, C.; Yang, Y.; Liu, B.; He, J.; Nie, Z. Polymer-guided assembly of inorganic nanoparticles. *Chem. Soc. Rev.* **2020**, *49*, 465−508.
(50) Liu, D.; Li, C.; Zhou, F.; Zhang, T.; Liu, G.; Cai, W.; Li, Y. Capillary Gradient-Induced Self-Assembly of Periodic Au Spherical Nanoparticle Arrays on an Ultralarge Scale via a Bisolvent System at Air/Water Interface. *Adv. Mater. Interfaces* **2017**, *4*, No. 1600976.
(51) Korgel, B. A.; Fullam, S.; Connolly, S.; Fitzmaurice, D. Assembly and Self-Organization of Silver Nanocrystal Superlattices: Ordered "Soft Spheres. *J. Phys. Chem. B* **1998**, *102*, 8379−8388.
(52) Whitney, A. V.; Elam, J. W.; Zou, S.; Zinovev, A. V.; Stair, P. C.; Schatz, G. C.; Duyne, R. P. V. Localized Surface Plasmon Resonance Nanosensor: A High-Resolution Distance-Dependence Study Using Atomic Layer Deposition. *J. Phys. Chem. B* **2005**, *109*, 20522−20528.
(53) Chow, T. H.; Li, N.; Bai, X.; Zhuo, X.; Shao, L.; Wang, J. Gold Nanobipyramids: An Emerging and Versatile Type of Plasmonic Nanoparticles. *Acc. Chem. Res.* **2019**, *52*, 2136−2146.

https://dx.doi.org/10.1021/acsami.0c01983
ACS Appl. Mater. Interfaces 2020, 12, 11296−11304